ACS OMEGA

http://pubs.acs.org/journal/acsodf

Article

Identification of the Intrinsic Motions and Related Key Residues Responsible for the Twofold Channel Opening of Poliovirus Capsid by Using an Elastic Network Model Combined with an Internal Coordinate

Jiao Li,[‖] Hao Zhang,[‖] Ning Liu, Yi Bo Ma, Wei Bu Wang, Qi Ming Li,* and Ji Guo Su*

Cite This: *ACS Omega* 2023, 8, 782−790

Read Online

ACCESS | Metrics & More | Article Recommendations

ABSTRACT: Poliovirus (PV) is an infectious virus that causes poliomyelitis, which seriously threatens the health of children. The release of viral RNA is a key step of PV in host cell infection, and multiple lines of evidence have demonstrated that RNA release is initiated by the opening of the twofold channels of the PV capsid. However, the mechanism that controls the twofold channel opening is still not well understood. In addition, the channel opening motion of the recombinant PV capsid leads to the destruction of predominant neutralizing epitopes and thus hinders the capsid as a vaccine immunogen. Therefore, it is important to identify the intrinsic motions and the related key residues controlling the twofold channel opening for understanding the virus infection mechanism and developing capsid-based vaccines. In the present work, the width of the channel was selected as an internal coordinate directly related to the channel opening, and then the elastic network model (ENM) combined with the group theory were employed to extract the intrinsic motion modes that mostly contribute to the opening of the twofold channels. Our results show that the channel opening predominately induced by the breathing motion and the overall rotation of each protomer in the capsid. Then, an internal coordinate-based perturbation method was used to identify the key residues regulating the twofold channel opening of PV. The calculation results showed that the predicted key residues are mainly located at the twofold axes, the bottom of the canyons and the quasi threefold axes. Our study is helpful for better understanding the twofold channel opening mechanism and provides a potential target for preventing the opening of the channels, which is of great significance for PV vaccine design. The source code of this study is available at https://github.com/SJGLAB/CapsidKeyRes.git.

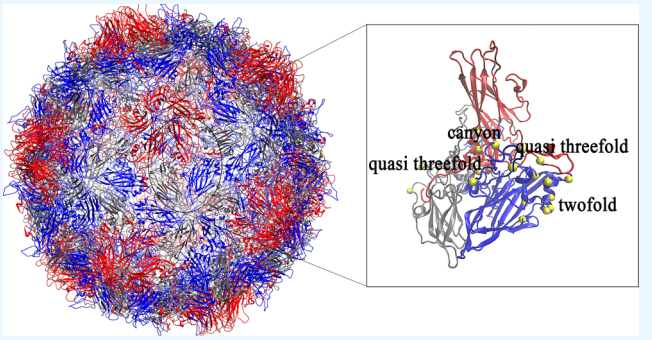

INTRODUCTION

Poliovirus (PV), as the causative agent of poliomyelitis (Polio), is a small and single-stranded positive RNA enterovirus, which causes paralysis or even death in children. PV is closely similar to several other important viruses, such as rhinovirus, coxsackieviruses, and hepatitis A virus.[1−5] PV invades the central nervous system, causing damage to the horn cells of the spinal cord, mainly through the digestive tract of the human body. The virus is extremely contagious and has spread to all parts of the world.[6] So far, great achievements have been made in PV vaccine development, and the live-attenuated oral Polio vaccine and the inactivated Polio vaccine have been widely used. However, the production of these vaccines requires the culture of live PV that faces the risk of virus release from the manufacturing workshop. The recombinant virus-like particle (VLP) vaccine, which can be manufactured without the culture of live virus, is a promising option to achieve the goal of global eradication of the PV.

The capsid of PV has an icosahedral symmetrical structure and is composed of 60 copies of units, each of which contains three coat proteins, that is, VP0, VP1, and VP3. In the mature viruses, VP0 is further cleaved into VP2 and VP4, and the virions become infectious virus particles.[2,7] VP1, VP2, and VP3 are similar in size, with about 30 kDa, and VP4 is relatively small, with about 7.5 kDa.[5] In the mature viruses, VP1, VP2, and VP3 have similar structures, each of which adopts an eight-

Received: September 22, 2022
Accepted: December 6, 2022
Published: December 16, 2022

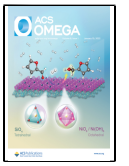

stranded β-barrel fold. VP1, VP2, and VP3 are located at the outside of the shell, and VP4 is inside the capsid, which stabilizes the capsid of the virus.[8] The PV capsid is highly symmetrical, which has 12 fivefold axes, 20 threefold axes, and 30 twofold axes. On the capsid, the fivefold symmetric rotation axes are located at the interface formed by five VP1s from adjacent protomers. The threefold symmetric rotation axes are situated at the interface formed by VP2 and VP3 from adjacent protomers. The twofold rotation axes are located at the channels formed by the alpha-helices of VP2 from the adjacent structural units.[9]

PV infection is triggered by the binding of the virus to the receptor of the host cell, and the receptor binding site in the capsid is located in the depths of the canyon surrounding the protrusion at the fivefold axes.[10,11] The attachment of the PV to the receptor causes a series of conformational transitions of the virus, which results in the changes in antigenicity.[12−14] The mature infectious virion (160S particle) is in the native D-antigen state. Receptor binding leads to the opening of the channels around the twofold and quasi threefold axes, through which the VP4 and N terminus of VP1 protruded out of the capsid to form the pore for RNA release.[15,16] Correspondingly, the virion is converted into the 135S particle. After release of viral RNA, the virus is changed into the 80S particle. Both 135S and 80S particles are C-antigenic forms. Numerous studies have revealed that only the D-antigen can elicit protective immune responses, but the C-antigen cannot induce immune protections.[17,18] The recombinant VLP of PV also inherently has a tendency of the opening of the twofold channels and correspondingly, the transition from D- to C-antigenic conformations, which results in the loss of neutralizing immunogenicity and thus hinders the recombinant VLP as an effective immunogen. Therefore, how to stabilize the capsid at the D-antigenic form and prevent the opening of the twofold channels are of significance for the recombinant VLP vaccine development. However, the molecular mechanism and the related key sites in controlling the opening of the twofold channels are still unclear.

In this work, the width of the twofold channel was used as a function-related internal coordinate, and the intrinsic motions mainly responsible for the twofold channel opening were analyzed by using the elastic network model (ENM) combined with the internal coordinate. Then, the key residues that control the opening of the twofold channels were identified by using a perturbation method based on the predefined function-related internal coordinate, in which the residues whose perturbation significantly altered the fluctuation of the internal coordinate were identified as the functionally key residues. According to the icosahedral symmetry of the PV capsid, the group theory was employed to reduce the computational costs in the normal mode calculations.

METHODS

ENM. The ENM simplifies each residue of the protein as a node located at its Cα atom and the interactions between residues were represented by springs with identical force constants. If the distance between the Cα atom of two residues is less than a cutoff radius, they are considered to be interacted and then connected by a spring. Otherwise, there is no spring between them.[19,20] In this work, the cutoff radius was selected as 12 Å. Then, the total potential energy of the system can be expressed as[21]

$$V = \frac{\gamma}{2}\sum_{i=1}^{N}\sum_{j>i}^{N}\tau_{ij}(R_{ij} - R_{ij}^{0})^2 = \frac{1}{2}[\Delta R^T H \Delta R] \tag{1}$$

where γ is the force constant of the springs; $\tau_{ij} = 1$ means that there is a spring between the ith and jth residues; $\tau_{ij} = 0$ means that there is no spring between them; R_{ij} and R_{ij}^0 are denoted as the instantaneous and equilibrium distances, respectively, between the ith and jth residues; ΔR represents the displacements of the protein residues from their equilibrium positions, which is a $3N$-dimensional column vector, and N is the number of residues in the protein; superscript T represents the transpose of the vector; and H is the $3N \times 3N$ dimensional Hessian matrix, which can be expressed in the following form

$$H = \begin{bmatrix} h_{11} & h_{12} & \cdots & h_{1N} \\ h_{21} & h_{22} & \cdots & h_{2N} \\ \vdots & \vdots & \vdots & \vdots \\ h_{N1} & h_{N2} & \cdots & h_{NN} \end{bmatrix} \tag{2}$$

where h_{ij} is a submatrix of 3×3 dimensions. The elements of h_{ij} are the second derivatives of the potential energy$V$, which can be calculated as

$$h_{ij} = \begin{bmatrix} \frac{\partial^2 V}{\partial X_i \partial X_j} & \frac{\partial^2 V}{\partial X_i \partial Y_j} & \frac{\partial^2 V}{\partial X_i \partial Z_j} \\ \frac{\partial^2 V}{\partial Y_i \partial X_j} & \frac{\partial^2 V}{\partial Y_i \partial Y_j} & \frac{\partial^2 V}{\partial Y_i \partial Z_j} \\ \frac{\partial^2 V}{\partial Z_i \partial X_j} & \frac{\partial^2 V}{\partial Z_i \partial Y_j} & \frac{\partial^2 V}{\partial Z_i \partial Z_j} \end{bmatrix} \tag{3}$$

where X_i, Y_i, and Z_i represent the three-dimensional Cartesian coordinates of the ith residue.

The diagonalization of Hessian matrix can obtain the eigenvectors and eigenvalues of the normal modes of the protein system. Based on these eigenvectors and eigenvalues, the mean-square fluctuation of the ith residue in the protein can be calculated by

$$\langle(\Delta R_i)^2\rangle = \frac{k_B T}{\gamma}(\langle(\Delta X_i)^2\rangle + \langle(\Delta Y_i)^2\rangle + \langle(\Delta Z_i)^2\rangle)$$

$$= \frac{k_B T}{\gamma}\sum_{k=7}^{3N}\frac{[v_k]_{3i-2}[v_k]_{3i-2} + [v_k]_{3i-1}[v_k]_{3i-1} + [v_k]_{3i}[v_k]_{3i}}{\lambda_k} \tag{4}$$

where k_B is the Boltzmann constant; T is the absolute temperature; γ is the force constant of the springs in ENM; k represents the kth normal mode; and v_k and λ_k are the eigenvector and eigenvalue of the kth normal mode, respectively. There are six modes with zero eigenvalue, which describe the overall translation and rotation of the system. These zero-eigenvalue modes have no contribution to the relative fluctuation of the residues in the protein and, thus, are excluded from the residue fluctuation calculation. The B-factor, also called Debye-Waller factor, of the ith residue can be computed as

$$B_i = \frac{8\pi^2}{3}\langle(\Delta R_i)^2\rangle$$

https://doi.org/10.1021/acsomega.2c06114
ACS Omega 2023, 8, 782−790

$$= \frac{8\pi^2 k_B T}{3\gamma} \sum_{k=7}^{3N} \frac{[v_k]_{3i-2}[v_k]_{3i-2} + [v_k]_{3i-1}[v_k]_{3i-1} + [v_k]_{3i}[v_k]_{3i}}{\lambda_k} \quad (5)$$

The cross correlation between the ith and jth residues can be calculated by

$$\langle \Delta R_i \bullet \Delta R_j \rangle = \frac{k_B T}{\gamma}(\langle \Delta X_i \bullet \Delta X_j \rangle + \langle \Delta Y_i \bullet \Delta Y_j \rangle + \langle \Delta Z_i \bullet \Delta Z_j \rangle)$$

$$= \frac{k_B T}{\gamma} \sum_{k=7}^{3N} \frac{[v_k]_{3i-2}[v_k]_{3j-2} + [v_k]_{3i-1}[v_k]_{3j-1} + [v_k]_{3i}[v_k]_{3j}}{\lambda_k} \quad (6)$$

However, the size of PV capsid is very large, and the diagonalization of the $3N \times 3N$ Hessian matrix is not a trivial task. Considering that the PV capsid has an icosahedral symmetry, which can be described by point group I, we used the group theory to reduce the dimension of the Hessian matrix and facilitate the calculation of the eigenvectors and eigenvalues of the normal modes.

Group Theory. The symmetry of the PV capsid is given by the point group I, which consists of 60 group elements. The point group I has five irreducible representations (irreps), that is, a1-dimensional representation A, a 3-dimensional T_1, a 3-dimensional T_2, a 4-dimensional G, and a 5-dimensional H.[22,23] According to the group theory, the Hessian matrix with the size of $60\mathcal{N} \times 60\mathcal{N}$ for the system, where $\mathcal{N}$ is the degree of freedom for each protomer of PV, can be block diagonalized into a series of sub-matrices with the size of $\mathcal{N} \times \mathcal{N}$, $3\mathcal{N} \times 3\mathcal{N}$, $3\mathcal{N} \times 3\mathcal{N}$, $4\mathcal{N} \times 4\mathcal{N}$, and $5\mathcal{N} \times 5\mathcal{N}$, respectively, in the irreps spaces. Based on the orthogonality theorem for the characters of the representations, the number of these five sub-matrices is 1, 3, 3, 4, and 5, respectively. Therefore, the utilizing group theory, the diagonalization of the high-dimensional Hessian matrix can be simplified into the diagonalization of a series of low-dimensional submatrices and thus, the computation cost and memory consuming can be significantly reduced.

To realize the block diagonalization of Hessian matrix, the basis functions of the irreps spaces were constructed by using the projection operator, which can be expressed as

$$\hat{P}^{p}_{st} = \sum_{g \in G} \tau^{p*}_{st}(g) T(g), \quad s, \quad t = 1, \ldots, s_p \quad (7)$$

where $\tau^{p}_{st}(g)$ represents the sth row and tth column of the pth irrep representation matrix; s_p is the dimension of the pth irrep representation matrix; the symbol "*" indicates complex conjugation; $T(g)$ is the representation matrix in the configuration space; and G represents the point symmetry group of PV and g is the element of the group G. Appling $\hat{P}^{p}_{st}$ on an arbitrary function $\vec{U}_k$ in the configuration space, we can obtain the basis functions of the irrep space $\vec{\phi}^{\,p,s}_k$, that is

$$\vec{\phi}^{\,p,s}_k = \hat{P}^{p}_{st} \vec{U}_k \quad (8)$$

$\vec{U}_k$ can be chosen as the basis functions of the configuration sub-space for the first protomer of PV, which can be expressed as $\vec{U}_k = (\vec{u}_k, 0, \ldots, 0)$, $k = 1,2,3, \ldots, \mathcal{N}$. Then, in the irreps spaces, Hessian matrix H can be block diagonalized, whose elements can be calculated as

$$\mathcal{H}^{ps,\lambda\sigma}_{k,\kappa} = {}^{t}\vec{\phi}^{\,p,s}_k H \vec{\phi}^{\,\lambda,\sigma*}_k = {}^{t}\vec{u}_k \left[\frac{n_G}{s_p} \sum_{M=1}^{n_G} \tau^{p}_{s\sigma}(M) H_{1M} T(M) \right] \vec{u}_\kappa \delta_{s\sigma} \delta_{p\lambda} \quad (9)$$

where n_G is the number of protomers in PV, which is equal to the order of group G; $T(M)$ is the symmetric transformation matrix from the first protomer to the Mth protomer; H_{1M} represents the sub-block of the Hessian matrix describing the interactions between the first and the Mth protomers; $\delta_{s\sigma}$ is equal to 1 for $s = \sigma$ or 0 for $s \neq \sigma$, and the same for $\delta_{p\lambda}$.

Through diagonalization of the series of matrix blocks given in eq 9 in the irreps spaces, the eigenvalues and eigenvectors were obtained. The eigenvalues calculated in the irreps spaces are the same as those in the configuration space. The eigenvectors obtained in the irreps spaces can be transformed into the configuration space by using the following formula, that is

$$\vec{y}^{\,j}_i = \sum_{s=1}^{s_p} \tau^{p}_{1s}(g_j) T(g_j) \sum_{k=\text{the}}^{N} \vec{u}_k z^{p}_{i,k} \quad (10)$$

where $\vec{y}^{\,j}_i$ is the eigenvector in the Cartesian coordinates for the jth protomer in the ith symmetry normal mode of the pth irrep; g_j is the symmetric operation that transforms the coordinates of protomer 1 to those of protomer j; and $z^{p}_{i,k}$ represents the kth entry of the ith normal mode in the pth irrep space.

Perturbation Method Based on a Predefined Internal Coordinate to Identify the Functionally Key Sites. Many previous studies have demonstrated that the opening of the twofold channel is essential for PV infections, from which the VP4 and the N-terminus of VP1 are externalized for genome release. In the PV capsid, the twofold channel is formed by two alpha-helices from adjacent VP2 subunits and thus, in this study, the width of the channel was described by the distance between the centroids of the two helices. The entire PV capsid contains totally contains 30 copies of the twofold channel. The average centroid distance of the 30 channels was used as the functionally related internal coordinate. In each subunit, the alpha-helix is composed of 10 residues, that is, MetT158, Gly159, Leu160, Phe161, Gly162, Gln163, Asn164, Met165, Tyr166, and Tyr167. Let the centroid of the 10 residues in a VP2 subunit be represented by P, and the centroid of the 10 residues in the corresponding adjacent VP2 subunit be denoted as Q. The centroid distance between P and Q can be written as

$$D_1 = \sqrt{(X_P - X_Q)^2 + (Y_P - Y_Q)^2 + (Z_P - Z_Q)^2} \quad (11)$$

For the 30 twofold channels, a total of 30 centroid distances were calculated, which were represented by $D_1, D_2, D_3, \ldots D_{28}, D_{29}$, and D_{30}, respectively. Then, the average width of the 30 twofold channels can be computed as $\bar{D} = \frac{(D_1 + D_2 + D_3 + \ldots + D_{28} + D_{29} + D_{30})}{30}$.

Under linear approximation, the fluctuation of the average width of the twofold channels in response to residue movements can be calculated as

https://doi.org/10.1021/acsomega.2c06114
ACS Omega 2023, 8, 782−790

$$\Delta\bar{D} = \sum_{i=1}^{N} \frac{\partial\bar{D}}{\partial X_i}\Delta X_i + \frac{\partial\bar{D}}{\partial Y_i}\Delta Y_i + \frac{\partial\bar{D}}{\partial Z_i}\Delta Z_i \quad (12)$$

where X_i, Y_i, and Z_i represent the three-dimensional Cartesian coordinates of the ith residue and N is the total number of residues in the capsid.

To identify the key sites involved in the opening of the twofold channels, the residues in the capsid were perturbed one by one, and the changes in the mean square fluctuation (MSF) of the function-related internal coordinate in response to the perturbations were calculated. Upon the perturbation of a residue, all the springs connecting to the residue were altered by changing their force constant. Then, the change in the MSF of the internal coordinate $\delta(\langle(\Delta\bar{D})^2\rangle)$ in response to the perturbation of a spring can expressed as

$$\delta(\langle(\Delta\bar{D})^2\rangle) = \frac{\partial\langle(\Delta\bar{D})^2\rangle}{\partial\gamma_{ij}}\Delta\gamma_{ij} \quad (13)$$

where $\Delta\gamma_{ij}$ is the change in the force constant of the spring between the ith and jth residues. $\frac{\partial\langle(\Delta\bar{D})^2\rangle}{\partial\gamma_{ij}}$ can be calculated according to the following formula[21]

$$\frac{\partial\langle(\Delta\bar{D})^2\rangle}{\partial\gamma_{ij}} = -\frac{1}{k_B T}(\langle\Delta\bar{D}\Delta R_{ij}\rangle)^2$$

$$= -\frac{1}{k_B T}\left(\frac{X_i^0 - X_j^0}{R_{ij}^0}\langle\Delta\bar{D}\Delta X_i\rangle + \frac{Y_i^0 - Y_j^0}{R_{ij}^0}\langle\Delta\bar{D}\Delta Y_i\rangle + \frac{Z_i^0 - Z_j^0}{R_{ij}^0}\langle\Delta\bar{D}\Delta Z_i\rangle - \frac{X_i^0 - X_j^0}{R_{ij}^0}\langle\Delta\bar{D}\Delta X_j\rangle - \frac{Y_i^0 - Y_j^0}{R_{ij}^0}\langle\Delta\bar{D}\Delta Y_j\rangle - \frac{Z_i^0 - Z_j^0}{R_{ij}^0}\langle\Delta\bar{D}\Delta Z_j\rangle\right)^2 \quad (14)$$

where k_B is the Boltzmann constant; T is the absolute temperature; R_{ij}^0 is the distance between the ith and jth residues at the equilibrium position; X_i^0, Y_i^0, and Z_i^0 are the Cartesian coordinates of the equilibrium position of the ith residue, and ΔX_i, ΔY_i, and ΔZ_i are the displacements of the ith residue. In our perturbation method, the residues whose perturbation significantly changes the value of $\delta(\langle(\Delta\bar{D})^2\rangle)$ were determined as the key residues controlling the opening of the twofold channels of PV. According to the normal modes obtained by the ENM combined with the group theory, the $\delta(\langle(\Delta\bar{D})^2\rangle)$ value can be calculated by eq 14 combined with eqs 4, 6 and 12.

RESULTS AND DISCUSSION

Comparison of the Calculated B-Factors of the Residues in the PV Capsid with the Experimental Data and the Molecular Dynamics Simulation Results. In this study, the nature empty PV particle (PDB no: 1POV) was studied by using the ENM combined with the group theory and the internal coordinate-based perturbation method. The nature empty capsids does not contain the viral RNA, and the capsid precursor protein VP0 is not cleaved into VP2 and VP4.[5] The PV capsid is an icosahedral symmetric structure composed of 60 copies of VP0, VP1, and VP3 proteins, with a diameter of 300 Å. The capsid structure is shown in Figure 1a,

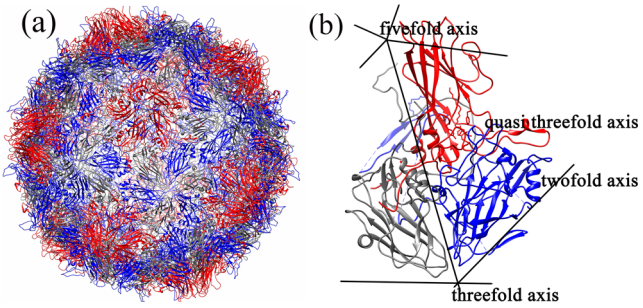

Figure 1. (a) Icosahedral symmetric structure of the PV capsid. The structural proteins VP0, VP1, and VP3 are displayed in blue, red, and gray colors, respectively. (b) Structure of a PV protomer. The locations of the fivefold, threefold, twofold, and quasi threefold axes are marked in the figure.

in which the VP0, VP1, and VP3 are displayed in blue, red, and gray colors, respectively. The symmetrical axes of the PV capsid, including the fivefold axis, twofold axis, threefold axis, and quasi threefold axis are marked in Figure 1b.

In order to verify the effectiveness of the ENM combined with the group theory to extract the intrinsic motions encoded in the capsid of PV, the B-factors of the residues in the system were first calculated by using eq 5, and the calculation results were compared with the experimental data and the MSF of the residues obtained by molecular dynamics (MD) simulation, as shown in Figure 2. The experimental B-factors were taken from

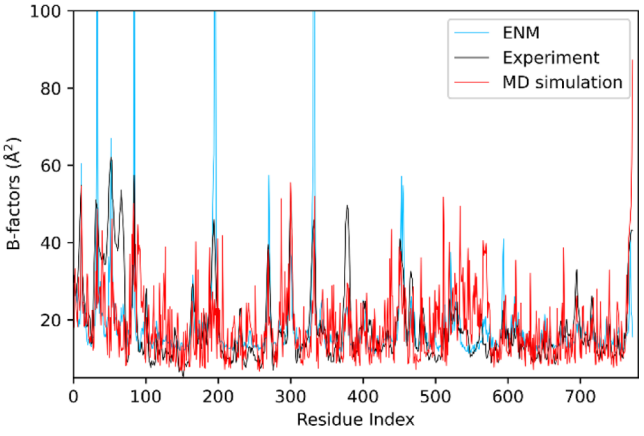

Figure 2. Comparison of the calculated B-factors (blue curve) of the residues in the PV capsid with the experimental data (black curve) and the molecular dynamics (MD) simulation results (red curve). It should be noted that the MSF profile obtained by MD simulations in different protomers is slightly varied, and only one protomer was shown in the figure.

the PDB file with the accession no. 1POV. The MD simulation was carried out by using GROMACS 2022 with the MARTINI elastic network (ELNEDYN) model.[24,25] The results show that the ENM combined group theory can well reproduce the experimental B-factors and the MD simulation results, indicating that our method is effective for investigating the intrinsic dynamics of PV capsid.

https://doi.org/10.1021/acsomega.2c06114
ACS Omega 2023, 8, 782−790

Internal Motion Modes Responsible for the Opening of the Twofold Channels on PV Capsid. Many studies have indicated that the opening of the twofold channels plays important roles in the infection of PV to host cells and also affects the immunological characteristics of the viral capsid.[15,26−28] The twofold channel in the capsid is formed by two helices of VP0 from the adjacent subunits and there are a total of 30 twofold channels in the PV capsid. Therefore, in the present work, the average centroid distance between the corresponding two helices of all the 30 channels was chosen as the function-related internal coordinate. Then, the intrinsic motion modes of PV capsid that predominantly contribute to the opening of the twofold channels were analyzed by using the internal-coordinate-based ENM combined with the group theory.

Employing the group theory, a total of 139,134 motion modes were obtained by using the ENM. However, these motion modes are not necessarily related to the opening of the twofold channels of PV. In this study, the normal modes with the large mean-square fluctuation (MSF) of the internal coordinate $\langle(\Delta\bar{D})^2\rangle$ were selected, which mainly contribute to the channel opening. Table 1 shows the first three modes with the largest $\langle(\Delta\bar{D})^2\rangle$ values. All these three modes belong to the irrep A and are nondegenerate. The motion modes of irrep A follow the icosahedral symmetry of the PV capsid structure, and the motions of the 60 symmetric units are identical.

Table 1. First Three Motion Modes That Dominantly Contribute to the Opening of the Twofold Channels on the PV Capsid

no.	irrep	eigenvalue	$\langle(\Delta\bar{D})^2\rangle^a$
1	A	8.97	6.37×10^{-2}
2	A	14.59	3.98×10^{-2}
3	A	3.99	2.57×10^{-2}

[a]The unit of $\langle(\Delta\bar{D})^2\rangle$ is $\frac{k_B T}{\gamma}$.

The three modes mostly contributing to the opening of the twofold channels are displayed in Figure 3. The first mode with the largest $\langle(\Delta\bar{D})^2\rangle$ is shown in Figure 3a. In this mode, the capsid expands along the radial direction, which is a typical breathing motion. This result indicates that along with the opening of the twofold channels, the capsid is uncoated. Numerous computational and experimental studies have also shown that the capsid uncoating of many viruses, such as PV,[29,30] rhinovirus,[31] and cowpea chlorotic mottle virus (CCMV),[32] leads to the opening of the twofold channels and then facilitates the release of viral RNA. Figure 3b shows the second motion mode mostly responsible for the twofold channel opening, which represents an overall rotation of each protomer around the axis at the bottom of the canyon. This motion results in the collapse of the regions around the fivefold axes and expansion outward of the regions around the twofold and quasi threefold axes. A similar rotation motion has also been observed in the intrinsic motions of other virus capsids, for example, enterovirus 71(EV71)[33] and coxsackievirus A16(CVA16).[34] The third motion mode that mostly contributes to the opening of the twofold channels is shown in Figure 3c. In this motion, each protomer as a whole undergoes a rotation motion approximately along the tangential direction of the capsid surface, and this motion leads to the obvious opening of the twofold channels. In addition, this mode also causes the open-closed motion of the canyon.

Identification of Key Residues Controlling the Opening of the Twofold Channels on PV Capsid. The key residues that control the opening of the twofold channels were identified by using an internal coordinate-based perturbation method. Considering the symmetry of the PV capsid, only the residues in the first protomer were perturbed one by one. The same results could be obtained for the perturbation of other protomers. In our method, residue perturbation was performed by altering the force constant of the springs connected to the residue, and then the MSF of the internal coordinate in response to the perturbation was calculated by using eq 14. The calculation result is shown in Figure 4. It is found that

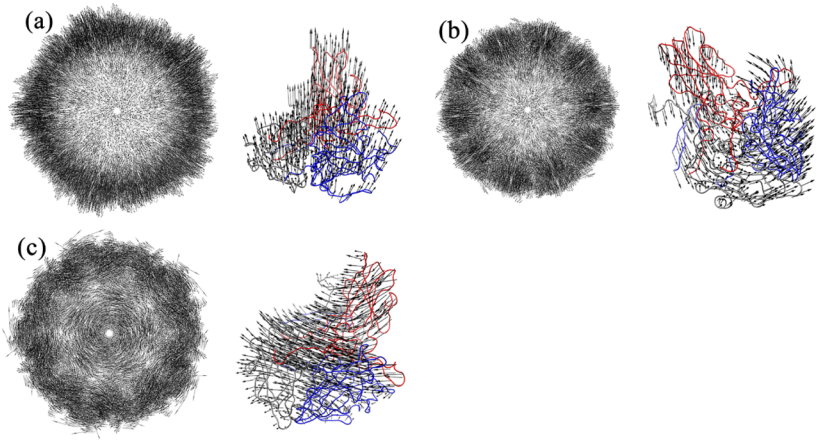

Figure 3. First three motion modes that mostly contribute the opening of the twofold channels on the PV capsid. (a−c) Modes with the first, second, and third largest $\langle(\Delta\bar{D})^2\rangle$, respectively. All these three modes belong to irrep A, and in each mode all the protomers of the capsid undergo the same motions. In each panel, the left sub-figure displays the motions of the whole capsid, and the right one shows the motions of any one protomer. The three chains of each protomer, that is, VP0, VP1, and VP3, are displayed in blue, red, and gray colors, respectively. In these figures, the length of the black arrows represents the relative amplitude of the displacement, and the direction of the displacement is determined by the direction indicated by the arrow.

https://doi.org/10.1021/acsomega.2c06114
ACS Omega 2023, 8, 782−790

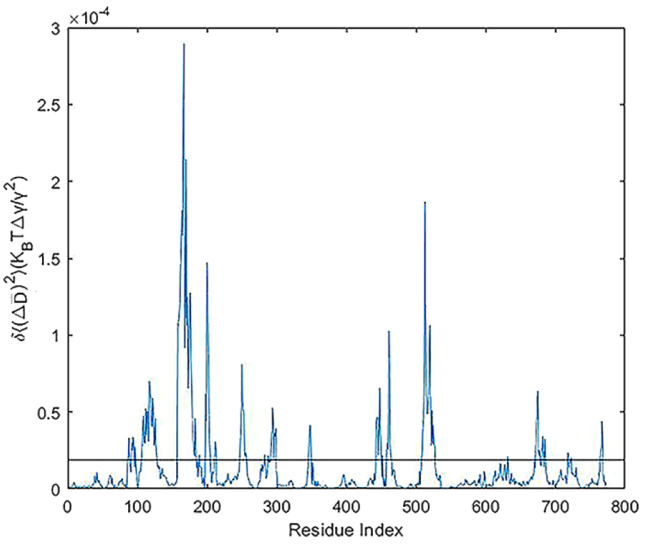

Figure 4. $\delta(\langle(\Delta\overline{D})^2\rangle)$ value in response to the perturbation of each residue in one of the protomers of PV capsid. The horizontal black line indicates the $\delta(\langle(\Delta\overline{D})^2\rangle)$ value of 2.0 × $\frac{10^{-5}K_BT\Delta\gamma}{\gamma^2}$. In the figure, only the calculation results for one protomer are shown, and the same results could be obtained for other protomers.

there are 18 clusters of residues whose $\delta(\langle(\Delta\overline{D})^2\rangle)$ values are larger than 2.0 × $\frac{10^{-5}K_BT\Delta\gamma}{\gamma^2}$, and the residues corresponding to the peak values of these clusters were identified as the functionally key residues. These residues predominately control the opening of the twofold channels on PV capsid.

Location of the Identified Key Residues on PV Capsid. According to the location in the tertiary structure of the PV capsid, the 18 key residues predicted by our method can be classified into three groups, as listed in Table 2. To visually display the location of these key residues, they are mapped onto the three-dimensional structure of one protomer of PV capsid, as shown in Figure 5.

Table 2. Key Residues That Regulate the Twofold Channel Opening Identified by the Internal Coordinate-Based Perturbation Method

key residue groups	key residues	locations
group 1	VP0: Leu135, Met158, Leu160, Gln163, Thr208, Pro324	the twofold channel
group 2	VP0: Phe230, Arg241, Gly253, VP1: Thr115, Tyr280	the bottom of the canyon
group 3	VP0: Val291, Ile335, Leu340	the quasi threefold channel
	VP1: Val215, Leu228	
	VP3: Asp140, Ser183	

The key residues of group 1, including Leu135, Met158, Leu160, Gln163, Thr208, and Pro324 of VP0, is located at the helix that is involved in the formation of the twofold channel. It is obvious that the residues in the helix mostly control the opening of the twofold channel. Strengthening the interactions between the two helices at the opposite sides of the twofold channel may be a direct yet effective method to prevent the opening of the channel. As discussed above, the opening of the twofold channel is coupled with the uncoating of PV capsid.

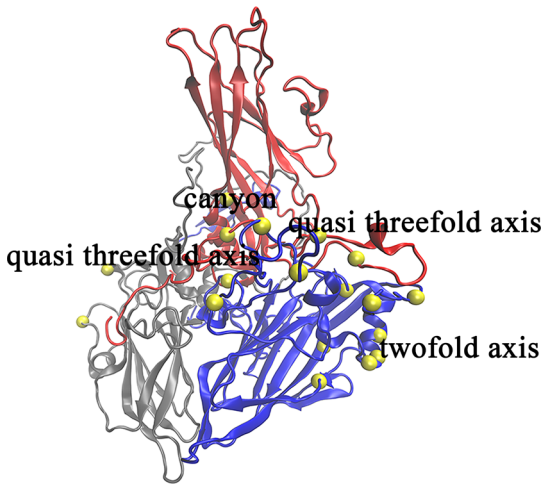

Figure 5. Location of the key residues that regulate the twofold channel opening identified by the internal coordinate-based perturbation method. The three chains VP0, VP1, and VP3 are displayed in blue, red, and gray colors, respectively, and the predicted key residues are displayed in yellow balls. In this figure, only one protomer was displayed, and the same results were obtained for other protomers.

Therefore, the stabilization of the channel in its closed conformation may also prevent the uncoating of the capsid and maintain its D-antigen state with immunological activity. The structural studies demonstrated that the twofold channels were distinctly expanded for the release of the viral RNA from PV capsids.[16] Several mutation experiments showed that introducing stronger inter-residue interactions, for example, disulfide bonds, electrostatic or hydrophobic interactions, across the twofold channel significantly improved the stability of the capsid of the foot-mouth disease virus, another picornavirus similar to PV, and prevented its expansion motions.[35−37]

The key residues of group 2 are located at the bottom of the canyon surrounding the fivefold axis, which include the residues Phe230, Arg241, and Gly253 from VP0 and Thr115 and Tyr280 from VP1. This region is also the binding site for the cellular receptor.[10,11] Several studies have demonstrated that receptor binding induces the squeeze of a fatty molecule from the hydrophobic pocket at the base of the canyon. The release of the fatty molecule causes the collapse of the hydrophobic pocket, which then triggers the opening of the twofold channels along with the uncoating of the capsid.[18,38,39] Therefore, the conformational changes in the canyon region are suggested to be coupled with the motions of the twofold channel through a long-range regulation. Our results also show that the key sites in the bottom of the canyon allosterically control the opening of the twofold channel, which is consistent with the previous studies discussed above. Fox et al. also shows that some mutations that stabilize the PV capsid in the unexpansive conformation existed in the canyon region.[40] The study of He et al. also revealed that several sites in the canyon region significantly regulated the uncoating of coxsackievirus A16 capsid.[34] Reisdorph et al. found that the mobility of the canyon region is critical for the capsid uncoating of rhinovirus, which is structurally similar to PV, and the binding of antiviral drugs or residue mutations in this region can block the functional motions of the virus.[41]

The key sites of group 3 are located at the region across the quasi threefold channel of the PV capsid, including the residues

https://doi.org/10.1021/acsomega.2c06114
ACS Omega 2023, 8, 782−790

Val291, Ile335, and Leu340 from VP0, Val215 and Leu228 from VP1, and Asp140, Ser183 from VP3. Several structural studies have indicated that the opening of the twofold channel further induced the expansion of the quasi threefold channel, through which the VP4 and terminus of VP1 exist out of the capsid.[40,42−45] Therefore, the opening of the twofold channel is accompanied by the opening of the quasi threefold channel. Multiple neutralizing antibody epitopes are situated at this region, and thus the conformational changes in the quasi threefold channel may destroy these epitopes and attenuate the immunogenicity of the capsid.[26,39,46,47] The study of Fox et al. also found that several stabilization mutations that could prevent the uncoating of PV are located at the quasi threefold channel.[40] Our calculation results agree with the observation of the previous studies.[40,48]

CONCLUSIONS

PV is a highly contagious virus, which seriously threatens the health of children. The opening of the twofold channels on the PV capsid is an essential step for viral RNA release and infection to host cells. The channel opening along with the associated uncoating of the capsid also significantly influences the immunogenicity of the virion. Therefore, preventing the twofold channel opening is an effective strategy for anti-virus drug design and VLP-based vaccine development. However, the intrinsic motions responsible for the opening of the channel and the related key residues controlling these motions are not well understood. In this work, the intrinsic motion modes of the PV capsid that mostly contribute to the opening of the twofold channels were studied by using the ENM combined with the group theory and then the key residues that predominately control the channel opening were identified by using a perturbation method based on a functionally related internal coordinate.

Our calculation results show that the first motion mode mostly contributing to the twofold channel opening is a breathing motion of the capsid. This motion causes the uncoating of the capsid along with the opening of the channel. The second- and third-most important motions are overall rotations of each protomer around different axes, both of which lead to the distinct expansion of the twofold channels. Then, a total of 18 key residues that predominately control the twofold channel opening were identified by using a perturbation method. These key residues were classified into three groups. Group 1 is located at the helices on the opposite sides of the twofold channel. Group 2 is located at the bottom of the canyon around the fivefold axes, and the key residues of group 3 are situated at the region across the quasi threefold channel. These key residues play important roles in the opening of the twofold channels as well as the uncoating of the capsid. The opening of the twofold channel is a key step for the infection of PV to the host cells. The identified key sites controlling the channel opening may serve as potential targets for anti-viral drug design to block the infection cycle of the virus. In addition, the channel opening and the associated capsid uncoating motions destroy the neutralizing epitopes and reduce the immunogenicity of the capsid. These key sites also provide promising targets for preventing the opening of the channels and maintaining the native immunogenic state, which enable the capsid to serve as an effective candidate for vaccine development against PV.

AUTHOR INFORMATION

Corresponding Authors

Qi Ming Li − *National Engineering Center for New Vaccine Research, Beijing 101111, China; The Sixth Laboratory, National Vaccine and Serum Institute (NVSI), Beijing 101111, China*; Email: liqiming189@163.com

Ji Guo Su − *High Performance Computing Center, National Vaccine and Serum Institute (NVSI), Beijing 101111, China; National Engineering Center for New Vaccine Research, Beijing 101111, China*; Email: jiguosu@hotmail.com

Authors

Jiao Li − *High Performance Computing Center, National Vaccine and Serum Institute (NVSI), Beijing 101111, China; National Engineering Center for New Vaccine Research, Beijing 101111, China*; orcid.org/0000-0003-0363-7018

Hao Zhang − *National Engineering Center for New Vaccine Research, Beijing 101111, China; The Sixth Laboratory, National Vaccine and Serum Institute (NVSI), Beijing 101111, China*

Ning Liu − *National Engineering Center for New Vaccine Research, Beijing 101111, China; The Sixth Laboratory, National Vaccine and Serum Institute (NVSI), Beijing 101111, China*

Yi Bo Ma − *High Performance Computing Center, National Vaccine and Serum Institute (NVSI), Beijing 101111, China; National Engineering Center for New Vaccine Research, Beijing 101111, China*

Wei Bu Wang − *High Performance Computing Center, National Vaccine and Serum Institute (NVSI), Beijing 101111, China; National Engineering Center for New Vaccine Research, Beijing 101111, China*

Complete contact information is available at: https://pubs.acs.org/10.1021/acsomega.2c06114

Author Contributions

‖J.L. and H.Z. contribute equally.

Notes

The authors declare no competing financial interest.

ACKNOWLEDGMENTS

This work was supported by the National Vaccine and Serum Institute (KTZC1900921A and KTZC1900014A).

REFERENCES

(1) Hobson, S. D.; Rosenblum, E. S.; Richards, O. C.; Richmond, K.; Kirkegaard, K.; Schultz, S. C. Oligomeric structures of poliovirus polymerase are important for function. *EMBO J.* **2001**, *20*, 1153−1163.

(2) Lentz, K. N.; Smith, A. D.; Geisler, S. C.; Cox, S.; Buontempo, P.; Skelton, A.; DeMartino, E.; Rozhon, E.; Schwartz, J.; Girijavallabhan, V.; O'Connell, J.; Arnold, E. Structure of poliovirus type 2 Lansing complexed with antiviral agent SCH48973: comparison of the structural and biological properties of the three poliovirus serotypes. *Structure* **1997**, *5*, 961−978.

(3) Smith, T. J.; Kremer, M. J.; Luo, M.; Vriend, G.; Arnold, E.; Kamer, G.; Rossmann, M. G.; McKinlay, M. A.; Diana, G. D.; Otto, M. J. The site of attachment in human rhinovirus 14 for antiviral agents that inhibit uncoating. *Science* **1986**, *233*, 1286−1293.

(4) Muckelbauer, J. K.; Kremer, M.; Minor, I.; Diana, G.; Dutko, F. J.; Groarke, J.; Pevear, D. C.; Rossmann, M. G. The structure of coxsackievirus B3 at 3.5 å resolution. *Structure* **1995**, *3*, 653−667.

(5) Basavappa, R.; Filman, D. J.; Syed, R.; Flore, O.; Icenogle, J. P.; Hogle, J. M. Role and mechanism of the maturation cleavage of VP0

https://doi.org/10.1021/acsomega.2c06114
ACS Omega 2023, 8, 782−790

in poliovirus assembly: Structure of the empty capsid assembly intermediate at 2.9 Å resolution. *Protein Sci.* **1994**, *3*, 1651−1669.
(6) Anis, E.; Kopel, E.; Singer, S. R.; Kaliner, E.; Moerman, L.; Moran-Gilad, J.; Sofer, D.; Manor, Y.; Shulman, L. M.; Mendelson, E.; Gdalevich, M.; Lev, B.; Gamzu, R.; Grotto, I. Insidious reintroduction of wild poliovirus into Israel, 2013. *Eurosurveillance* **2013**, *18*, 20586.
(7) Sonenberg, N. Regulation of translation by poliovirus. *Adv. Virus Res.* **1987**, *33*, 175−204.
(8) Chow, M.; Newman, J. F. E.; Filman, D.; Hogle, J. M.; Rowlands, D. J.; Brown, F. Myristylation of picornavirus capsid protein VP4 and its structural significance. *Nature* **1987**, *327*, 482−486.
(9) Hogle, J. M.; Chow, M.; Filman, D. J. Three-Dimensional Structure of Poliovirus at 2.9 Å Resolution. *Science* **1985**, *229*, 1358−1365.
(10) Belnap, D. M.; McDermott, B. M., Jr; Filman, D. J.; Cheng, N.; Trus, B. L.; Zuccola, H. J.; Racaniello, V. R.; Hogle, J. M.; Steven, A. C. Three-dimensional structure of poliovirus receptor bound to poliovirus. *Proc. Natl. Acad. Sci. U.S.A.* **2000**, *97*, 73−78.
(11) He, Y.; Mueller, S.; Chipman, P. R.; Bator, C. M.; Peng, X.; Bowman, V. D.; Mukhopadhyay, S.; Wimmer, E.; Kuhn, R. J.; Rossmann, M. G. Complexes of poliovirus serotypes with their common cellular receptor, CD155. *J. Virol.* **2003**, *77*, 4827−4835.
(12) Mendelsohn, C. L.; Wimmer, E.; Racaniello, V. R. Cellular receptor for poliovirus: molecular cloning, nucleotide sequence, and expression of a new member of the immunoglobulin superfamily. *Cell* **1989**, *56*, 855−865.
(13) Fenwick, M. L.; Cooper, P. D. Early interactions between poliovirus and ERK cells: some observations on the nature and significance of the rejected particles. *J. Virol.* **1962**, *18*, 212−223.
(14) De Sena, J.; Mandel, B. Studies on the in vitro uncoating of poliovirus II. Characteristics of the membrane-modified particle. *Virology* **1977**, *78*, 554−566.
(15) Bostina, M.; Levy, H.; Filman, D. J.; Hogle, J. M. Poliovirus RNA is released from the capsid near a twofold symmetry axis. *J. Virol.* **2011**, *85*, 776−783.
(16) Butan, C.; Filman, D. J.; Hogle, J. M. Cryo-electron microscopy reconstruction shows poliovirus 135S particles poised for membrane interaction and RNA release. *J. Virol.* **2014**, *88*, 1758−1770.
(17) Beale, A. J.; Mason, P. J. The measurement of the D-antigen in poliovirus preparations. *Epidemiol. Infect.* **1962**, *60*, 113−121.
(18) Strauss, M.; Schotte, L.; Thys, B.; Filman, D. J.; Hogle, J. M. Five of five VHHs neutralizing poliovirus bind the receptor-binding site. *J. Virol.* **2016**, *90*, 3496−3505.
(19) Su, J. G.; Jiao, X.; Sun, T. G.; Li, C. H.; Chen, W.; Wang, C. X. Analysis of domain movements in glutamine-binding protein with simple models. *Biophys. J.* **2007**, *92*, 1326−1335.
(20) Eyal, E.; Yang, L. W.; Bahar, I. Anisotropic network model: systematic evaluation and a new web interface. *Bioinformatics* **2006**, *22*, 2619−2627.
(21) Zhang, P. F.; Su, J. G. Identification of key sites controlling protein functional motions by using elastic network model combined with internal coordinates. *J. Chem. Phys.* **2019**, *151*, 045101.
(22) Hu, W. M.; Yong, J. L.; Zhou, J.; Shu, F. The irreducible representation matrices of the icosahedral point groups I and Ih. *Superlattices Microstruct.* **1987**, *3*, 391−398.
(23) van Vlijmen, H. W. T.; Karplus, M. Normal mode analysis of large systems with icosahedral symmetry: Application to (Dialanine)-60 in full and reduced basis set implementations. *J. Chem. Phys.* **2001**, *115*, 691−698.
(24) Periole, X.; Cavalli, M.; Marrink, S. J.; Ceruso, M. A. Combining an elastic network with a coarse-grained molecular force field: structure, dynamics, and intermolecular recognition. *J. Chem. Theory Comput.* **2009**, *5*, 2531−2543.
(25) Globisch, C.; Krishnamani, V.; Deserno, M.; Peter, C. Optimization of an elastic network augmented coarse grained model to study CCMV capsid deformation. *PLoS One* **2013**, *8*, No. e60582.
(26) Levy, H. C.; Bostina, M.; Filman, D. J.; Hogle, J. M. Catching a virus in the act of RNA release: a novel poliovirus uncoating intermediate characterized by cryo-electron microscopy. *J. Virol.* **2010**, *84*, 4426−4441.
(27) Garriga, D.; Pickl-Herk, A.; Luque, D.; Wruss, J.; Castón, J. R.; Blaas, D.; Verdaguer, N. Insights into minor group rhinovirus uncoating: the X-ray structure of the HRV2 empty capsid. *PLoS Pathog.* **2012**, *8*, No. e1002473.
(28) Shakeel, S.; Seitsonen, J. J.; Kajander, T.; Laurinmäki, P.; Hyypiä, T.; Susi, P.; Butcher, S. J. Structural and Functional Analysis of Coxsackievirus A9 Integrin α v β 6 Binding and Uncoating. *J. Virol.* **2013**, *87*, 3943−3951.
(29) Fricks, C. E.; Hogle, J. M. Cell-induced conformational change in poliovirus: externalization of the amino terminus of VP1 is responsible for liposome binding. *J. Virol.* **1990**, *64*, 1934−1945.
(30) Belnap, D. M.; Filman, D. J.; Trus, B. L.; Cheng, N.; Booy, F. P.; Conway, J. F.; Curry, S.; Hiremath, C. N.; Tsang, S. K.; Steven, A. C.; et al. Molecular tectonic model of virus structural transitions: the putative cell entry states of poliovirus. *J. Virol.* **2000**, *74*, 1342−1354.
(31) Hewat, E. A.; Neumann, E.; Blaas, D. The concerted conformational changes during human rhinovirus 2 uncoating. *Mol. Cell* **2002**, *10*, 317−326.
(32) Liu, H.; Qu, C.; Johnson, J. E.; Case, D. A. Pseudo-atomic models of swollen CCMV from cryo-electron microscopy data. *J. Struct. Biol.* **2003**, *142*, 356−363.
(33) Ross, C. J.; Atilgan, A. R.; Tastan Bishop, Ö. T.; Atilgan, C. Unraveling the motions behind enterovirus 71 uncoating. *Biophys. J.* **2018**, *114*, 822−838.
(34) He, X. L.; Du, L. F.; Zhang, J.; Liang, Y.; Wu, Y. D.; Su, J. G.; Li, Q. M. The functional motions and related key residues behind the uncoating of coxsackievirus A16. *Proteins* **2021**, *89*, 1365−1375.
(35) Porta, C.; Kotecha, A.; Burman, A.; Jackson, T.; Ren, J.; Loureiro, S.; Jones, I. M.; Fry, E. E.; Stuart, D. I.; Charleston, B. Rational engineering of recombinant picornavirus capsids to produce safe, protective vaccine antigen. *PLoS Pathog.* **2013**, *9*, No. e1003255.
(36) Mateo, R.; Luna, E.; Rincón, V.; Mateu, M. G. Engineering viable foot-and-mouth disease viruses with increased thermostability as a step in the development of improved vaccines. *J. Virol.* **2008**, *82*, 12232−12240.
(37) Kotecha, A.; Seago, J.; Scott, K.; Burman, A.; Loureiro, S.; Ren, J.; Porta, C.; Ginn, H. M.; Jackson, T.; Perez-Martin, D. I.; et al. Structure-based energetics of protein interfaces guides foot-and-mouth disease virus vaccine design. *Nat. Struct. Mol. Biol.* **2015**, *22*, 788−794.
(38) Filman, D. J.; Syed, R.; Chow, M.; Macadam, A. J.; Minor, P. D.; Hogle, J. M. Structural factors that control conformational transitions and serotype specificity in type 3 poliovirus. *EMBO J.* **1989**, *8*, 1567−1579.
(39) Strauss, M.; Filman, D. J.; Belnap, D. M.; Cheng, N.; Noel, R. T.; Hogle, J. M. Nectin-like interactions between poliovirus and its receptor trigger conformational changes associated with cell entry. *J. Virol.* **2015**, *89*, 4143−4157.
(40) Fox, H.; Knowlson, S.; Minor, P. D.; Macadam, A. J. Genetically thermo-stabilised, immunogenic poliovirus empty capsids; a strategy for non-replicating vaccines. *PLoS Pathog.* **2017**, *13*, No. e1006117.
(41) Reisdorph, N.; Thomas, J. J.; Katpally, U.; Chase, E.; Harris, K.; Siuzdak, G.; Smith, T. J. Human rhinovirus capsid dynamics is controlled by canyon flexibility. *Virology* **2003**, *314*, 34−44.
(42) Danthi, P.; Tosteson, M.; Li, Q. H.; Chow, M. Genome delivery and ion channel properties are altered in VP4 mutants of poliovirus. *J. Virol.* **2003**, *77*, 5266−5274.
(43) Smyth, M. S.; Martin, J. H. Picornavirus uncoating. *Mol. Pathol.* **2002**, *55*, 214.
(44) Wang, X.; Peng, W.; Ren, J.; Hu, Z.; Xu, J.; Lou, Z.; Li, Z.; Yin, X.; Shen, W.; Porta, X.; et al. A sensor-adaptor mechanism for enterovirus uncoating from structures of EV71. *Nat. Struct. Mol. Biol.* **2012**, *19*, 424−429.
(45) He, M.; Xu, L.; Zheng, Q.; Zhu, R.; Yin, Z.; Zha, Z.; Lin, Y.; Yang, L.; Huang, Y.; Ye, N.; et al. Identification of antibodies with

https://doi.org/10.1021/acsomega.2c06114
ACS Omega 2023, 8, 782−790

non-overlapping neutralization sites that target coxsackievirus A16. *Cell Host Microbe* **2020**, *27*, 249−261.
(46) Ren, J.; Wang, X.; Hu, Z.; Gao, Q.; Sun, Y.; Li, X.; Porta, C.; Walter, T. S.; Gilbert, R. J.; Fry, E. E.; et al. Picornavirus uncoating intermediate captured in atomic detail. *Nat. Commun.* **2013**, *4*, 1929.
(47) Lyu, K.; Ding, J.; Han, J. F.; Zhang, Y.; Wu, X. Y.; He, Y. L.; Qin, C. F.; Chen, R. Human enterovirus 71 uncoating captured at atomic resolution. *J. Virol.* **2014**, *88*, 3114−3126.
(48) Marsian, J.; Fox, H.; Bahar, M. W.; Kotecha, A.; Fry, E. E.; Stuart, D. I.; Macadam, A. J.; Rowlands, D. J.; Lomonossoff, G. P. Plant-made polio type 3 stabilized VLPs-a candidate synthetic polio vaccine. *Nat. Commun.* **2017**, *8*, 245−9.

https://doi.org/10.1021/acsomega.2c06114
ACS Omega 2023, 8, 782−790